Processing and Application of Ceramics 17 [4] (2023) 374–383
https://doi.org/10.2298/PAC2304374L

Study on process and parameter optimization of selective laser sintering of SiC composite powder

Jian Li[1,*], Xiao Liang[1], Yanling Guo[1], Yangwei Wang[1], Shuai Guo[1], Jianxun Bao[2], Wei Li[2]

[1]*College of Mechanical and Electrical Engineering, Northeast Forestry University, Harbin, China*
[2]*Changchun Institute of Optics, Fine Mechanics and Physics, Chinese Academy of Sciences, Changchun, China*

Received 14 June 2023; Received in revised form 24 October 2023; Accepted 25 November 2023

Abstract

This study aims to utilize silicon carbide (SiC) powder and phenol-formaldehyde resin (PF) as the primary raw materials to prepare phenol-formaldehyde coated silicon carbide composite (PCSC) using a thermal coating method. Then, single-factor experiment and orthogonal experiment were used to optimize the process parameters of selective laser sintering (SLS). Finally, SiC precursors were formed using optimized process parameters with excellent density and dimensional accuracies. The results show that the best combination of process parameters is: laser power of 25 W, scanning speed of 1.7 m/s, scanning spacing of 0.12 mm and layer thickness of 0.16 mm.

Keywords: *selective laser sintering, silicon carbide, orthogonal experiment, parameter optimization*

I. Introduction

With the rapid development of modern industrial technology, the fabrication techniques for ceramic-based composite materials have become a key focus of research for scholars worldwide [1]. Silicon carbide (SiC) finds applications in various fields, including high-power microwave equipment, high-temperature electronic/optical devices, sensors and optoelectronic detectors, owing to its exceptional properties [2,3]. These properties encompass high mechanical stiffness, low density, wide bandgap, low coefficient of thermal expansion, high thermal stability and corrosion resistance [4–6]. Over the years, conventional manufacturing processes have been successfully developed to fabricate intricate SiC parts since the 1990s [7]. Nonetheless, these processes possess certain limitations such as complex processing, high costs, and long manufacturing cycles. In specific applications, additive manufacturing (AM) holds significant advantages for producing intricate ceramic structures and it has garnered extensive research attention [8]. Compared to traditional manufacturing technologies, additive manufacturing eliminates geometric constraints during the shaping process, thereby having the potential to further expand the design possibilities of complex structures [9]. Similar to the industrial revolution triggered by steam engines and Ford assembly lines, additive manufacturing is also regarded as a transformative technology with the capacity to reshape the world, thus becoming a prominent research focus in the manufacturing industry. Numerous researchers have investigated the fabrication processes and component properties of SiC-based composite parts produced using various additive manufacturing techniques [10].

Selective laser sintering (SLS) is an AM technology that employs laser scanning to selectively sinter powder beds, enabling layer-by-layer fabrication [11,12]. It has been extensively utilized for manufacturing ceramic components based on SiC [13]. Compared with other 3D printing technologies, SLS technology has the advantages of having no support during processing, unsintered material can be reused and recycled, and a wide range of materials can be used [14]. Parts with complex structure can be printed directly through SLS by a simplified manufacturing process; meanwhile, the production time and costs are reduced [15,16]. In 1986, Carl R. Deckard defined selective laser sintering and proposed its applicability to various raw materials, including ceramics in powder form [17,18]. Gen-

*Corresponding author: tel: +86 15846144387,
e-mail: *lijian@nefu.edu.cn*

erally, the materials used in SLS are polycarbonate (PC) powder [19], polystyrene (PS) powder [20], phenol-formaldehyde (PF) powder [21], epoxy resin powder [22] and their derivative materials. SiC does not exist in liquid form under normal atmospheric conditions. Instead, it decomposes into liquid silicon and solid carbon at temperatures exceeding 2545 °C, making direct selective laser sintering of SiC unfeasible [23]. In 1995, the University of Texas at Austin conducted the first study on indirect SLS of SiC, which demonstrated that SiC ceramics could be formed by introducing low-melting-point binders and utilizing SLS technology [24]. Subsequent research focused on exploring different combinations of powders and binders to enhance the density and performance of SiC parts manufactured through indirect SLS. Zhu *et al.* [25] employed phenol-formaldehyde (PF) resin-coated carbon fibre (C_f) composite powder as raw materials and obtained C_f/SiC composites through SLS, vacuum resin infiltration, pyrolysis and liquid silicon infiltration. The overall linear shrinkage rate was below 3%, and the maximum density reached 2.80–2.86 g/cm^3 with a 10 vol.% content of PF. Liu *et al.* [26] used PF as a coating material for SiC particles and carbon black, resulting in SiC-PF-C composite powder. SLS, cold isostatic pressing and reactive sintering were employed to prepare SiC ceramics with an 18 wt.% content of PF, achieving a maximum density of 2.94–2.98 g/cm^3 for the reactive sintered body. Zhang *et al.* [8] utilized SiC and epoxy resin (E12) as raw materials to produce green bodies via SLS, followed by a precursor impregnation and pyrolysis (PIP) process, yielding SiC particle/SiC (SiC_p/SiC) composite lattice core sandwich panels. The density of the SiC_p/SiC composite material increased from 1.30 to 2.67 g/cm^3 after the PIP process. Song *et al.* [27] employed SiC, spherical graphite, silicon powder (Si) and E12 as raw materials, using a combination of SLS and a two-step sintering process to prepare SiC/Si composite materials, which effectively reduced the residual silicon content in the sintered body.

In summary, phenol-formaldehyde (PF) and epoxy resin (E12) have been extensively utilized as binders in the indirect SLS of SiC. Both binders require pyrolysis to convert into a carbon source for reaction sintering after SLS. However, E12's lower residual carbon content will lead to higher residual silicon content after reaction sintering. Although PF has higher residual carbon content, its higher shrinkage rate can cause significant size deviations during SLS, curing process and the carbonization pyrolysis reaction. To address these issues, this study employed a thermal coating method to prepare phenol-formaldehyde coated silicon carbide composite (PCSC) powder, reducing the PF content and minimizing size deviations and porosity in green parts. The effects of SLS process parameters on the density and dimensional accuracies in the *X*, *Y* and *Z* directions of the PCSC parts were investigated, and an orthogonal experimental design with four factors and four levels was employed to optimize the SLS process parameters. Finally, a kind of silicon carbide precursor with excellent density and dimensional accuracies was formed using optimized parameters.

II. Experimental

2.1. Raw materials and sample preparation

PCSC is mainly composed of SiC powder and PF powder, and two components accounted for more than 99 wt.%. There are also other additives in PCSC such as curing agent and lubricant.

The main raw material for SLS moulding was SiC powder (SiC >99 wt.%, Sanmenxia Xinfeng Abrasive Co. Ltd, Sanmenxia, China) with a particle size of $D_{97} < 60$ μm. During the SLS formation process, a phenol-formaldehyde (PF) resin (thermoplasticity 2123 type, Jinan Dahui Chemical Technology Co. Ltd, Jinan, China) was used as the low-melting-point binder. Hexamethylenetetramine ($C_6H_{12}N_4$ >99 wt.%, Sinopharm Chemical Reagent Co. Ltd, Shanghai, China) was employed as the curing agent, with the amount of 10 wt.% of PF. Calcium stearate ($C_{36}H_{70}CaO_4$ >99 wt.%, Hebei Baiyilian Chemical Technology Co. Ltd, Hebei, China) served as the lubricant, with the amount of 6 wt.% of PF.

When heated, hexamethylenetetramine breaks down and undergoes a solidification reaction with PF. This reaction can maintain the shape of the PCSC part during the post-processing reactions like carbonization.

This experiment employs a thermal coating method to apply a coating to SiC powder. The SiC powder is first heated at 190 °C for 1 h in a constant temperature furnace. It is then transferred to a SHY blade-type sand mixer for mixing and grinding, followed by cooling to 160 °C before adding PF powder for further mixing. Once the temperature drops to 120 °C, the preconfigured hexamethylenetetramine solution and calcium stearate are introduced and mixed. After cooling to 80 °C, the mixture is removed from the sand mixer and rapidly cooled to room temperature. Subsequently, the cooled mixture is crushed and agglomerated particles are eliminated using a 120 μm sieve, resulting in the production of PCSC with an actual phenol-formaldehyde resin content of 7 wt.%. Figure 1 illustrates the preparation processes of the PCSC.

The SLS experiment employed the CX-B200 rapid prototyping device (Harbin Free Intelligent Manufacturing Technology Development Co. Ltd, Harbin, China), which was equipped with a CO_2 laser generator. The laser generator had a wavelength of 10.6 μm and a power output of 40 W. The forming box had dimensions of 220 mm × 220 mm × 220 mm, and the forming speed could reach up to 3.5 m/s. The layer thickness varied from 0.08 mm to 0.4 mm and no protective atmosphere was utilized. 3D solid objects were produced by selective laser sintering of consecutive powder layers derived from computer-aided design models. The laser beam continuously fused the powder with the previous

layer. For a visual representation of the rapid prototyping device and the process, refer to Fig. 2. "Sintering" in this paper refers to joining SiC particles by molten and then solidified PF (a binder).

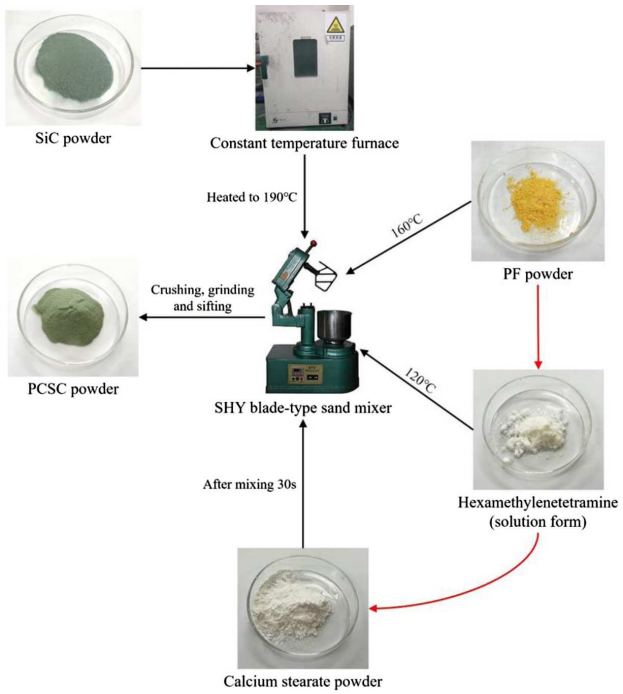

Figure 1. A flow chart of the preparation process of the PCSC powder

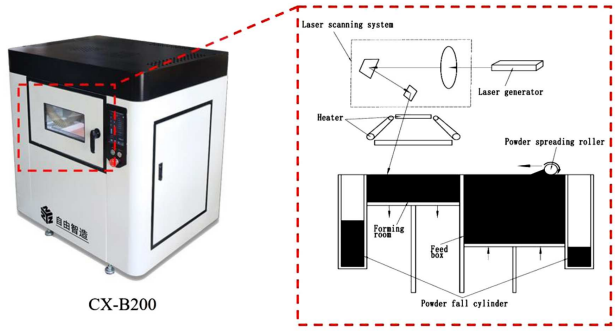

Figure 2. A flow chart of the selective laser sintering process

2.2. Orthogonal experiment design

The laser power, scanning speed, scanning spacing and layer thickness exert a substantial influence on the forming performance of parts during SLS processing. To conduct an orthogonal experiment effectively, it is crucial to ascertain the impact of each factor on the test results, thereby ensuring the feasibility of the orthogonal experiment. Table 1 presents the SLS process parameters.

The evaluation of formability in the SLS process requires careful consideration of the density and dimensional accuracy of PCSC parts. Given the intricate nature of SLS, these factors are dependent on the process parameters governing the sintered part. To investigate the impact of process parameters on the density and Z-direction dimensional accuracy of PCSC parts, a four-factor four-level orthogonal experimental design was employed during the SLS process test. This approach aimed to establish the formability principles of SLS. The experimental design for PCSC in SLS is presented in Table 2.

2.3. Testing and characterization

Morphologies of the SiC and PCSC powders were observed using the FEI Quanta 200 SEM (Hewlett-Packard Company, Amsterdam, The Netherlands). Figure 3 displays the morphology of the pristine SiC and PCSC powders. The SiC particles exhibit a well-defined and flat surface with distinct edges. However, after being coated with PF, they become rough and rounded, with some residual PF particles remaining on the surface.

The glass-transition temperature of PF powder was determined using a TA Instruments' TAQ200 model differential scanning calorimeter (DSC, Waters Technologies Ltd, Shanghai, China). The testing was conducted in a temperature range of 30 to 180 °C, with a heating rate of 10 °C/min, under a nitrogen gas atmosphere. The DSC curve of the PF powder is presented in Fig. 4.

The mass and dimensions of the PCSC samples were measured using an electronic balance and a calliper. The density was calculated using Eq. 1:

Table 1. SLS process parameters

factors	Laser power [W]	Scanning speed [m/s]	Scanning spacing [mm]	Layer thickness [mm]
$A_1/A_2/A_3/A_4$	24/25/26/27	1.5	0.10	0.15
$B_1/B_2/B_3/B_4$	27	1.4/1.5/1.6/1.7	0.10	0.15
$C_1/C_2/C_3/C_4$	27	1.5	0.10/0.11/0.12/0.13	0.15
$D_1/D_2/D_3/D_4$	27	1.5	0.10	0.13/0.14/0.15/0.16

Table 2. The factors and levels of SLS orthogonal experiment

Level	Laser power [W] A	Scanning speed [m/s] B	Scanning spacing [mm] C	Layer thickness [mm] D
1	23	1.4	0.1	0.13
2	24	1.5	0.11	0.14
3	25	1.6	0.12	0.15
4	26	1.7	0.13	0.16

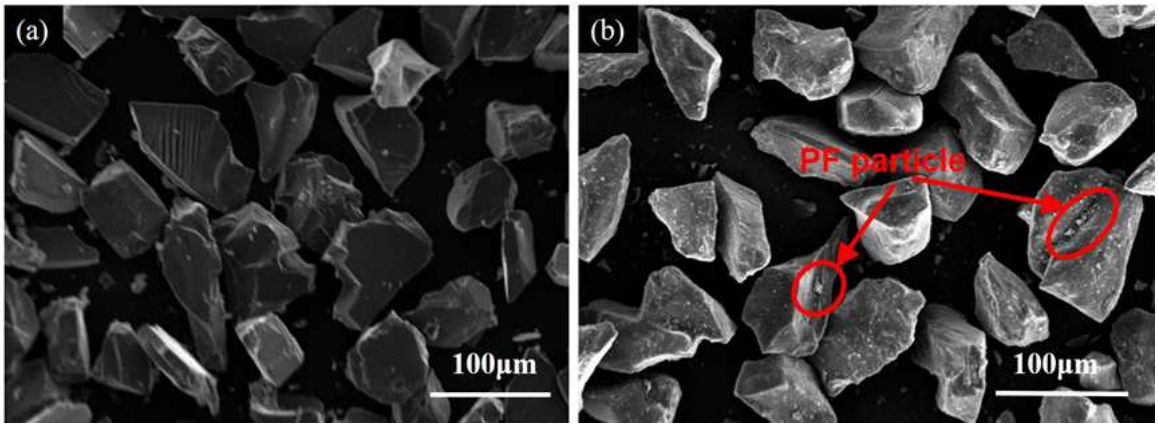

Figure 3. SEM images of: a) SiC and b) PCSC powders

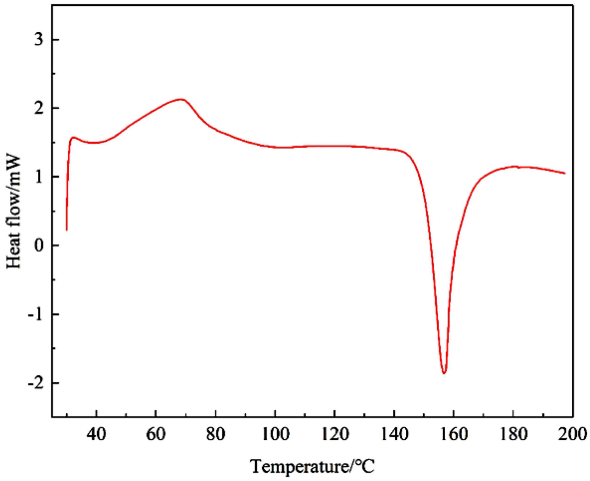

Figure 4. The DSC curve of the PF powder

$$\rho = \frac{W}{l \cdot b \cdot h} \tag{1}$$

where W represents the mass of parts, l denotes the length of parts, b represents the width of parts and h indicates the thickness of parts.

For the dimensional accuracy analysis, a cube sample with dimensions of 20 mm × 20 mm × 20 mm was utilized, as shown in Fig. 5. PCSC parts were manufactured using SLS with various process parameters (Table 1). The actual dimensions of the PCSC parts were measured using a vernier calliper. The dimensional accuracy δ, was calculated using Eq. 2:

$$\delta = 1 - \frac{|L_0 - L|}{L_0} \tag{2}$$

where δ represents the dimensional accuracy of parts, L_0 signifies the standard dimension of parts and L represents the actual dimension of parts. Additionally, the dimensions of the PCSC parts were measured in the X (the direction of the movement of the powder roller), Y and Z (the direction of the layer thickness) directions. The dimensional accuracies in the X, Y and Z directions, represented by δ_X, δ_Y and δ_Z, respectively, were also calculated.

III. Results and discussion

3.1. The preheating temperature

Figure 4 presents the DSC curve of the PF powder in the temperature range of 30 to 200 °C. The curve exhibits the endothermic peak occurring at 68.34 °C. From the DSC curve, the glass transition temperature of PF is determined to be 46.51 °C and this temperature is the estimated preheating temperature of the PCSC powder. After some previous sintering experiments, a suitable laser sintering preheating temperature of 70 °C is established for PCSC.

3.2. Single-factor analysis

A single-factor experiment was conducted to determine the impact of process parameters on the density and the dimensional accuracy of PCSC parts in the X, Y and Z directions. It should be pointed out that although PF shrinks when irradiated by laser, the actual dimensions of PCSC parts are larger than the nominal dimensions because the amount of added PF is small and the energy of laser transports to the surrounding powder, melting and sintering the PF in the surrounding powder together. Thus, higher dimensional accuracy corresponds to smaller dimensions, and vice versa.

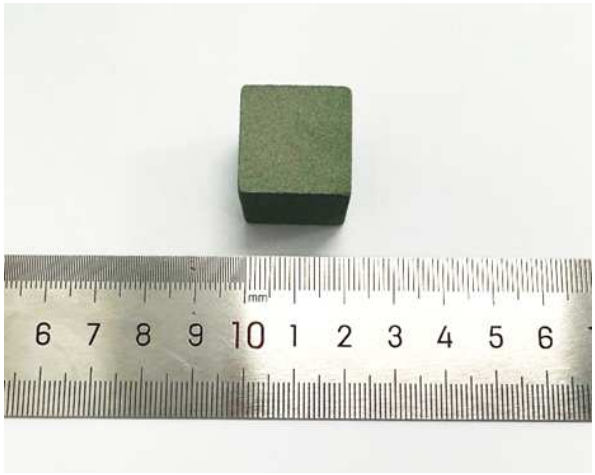

Figure 5. Cube sample

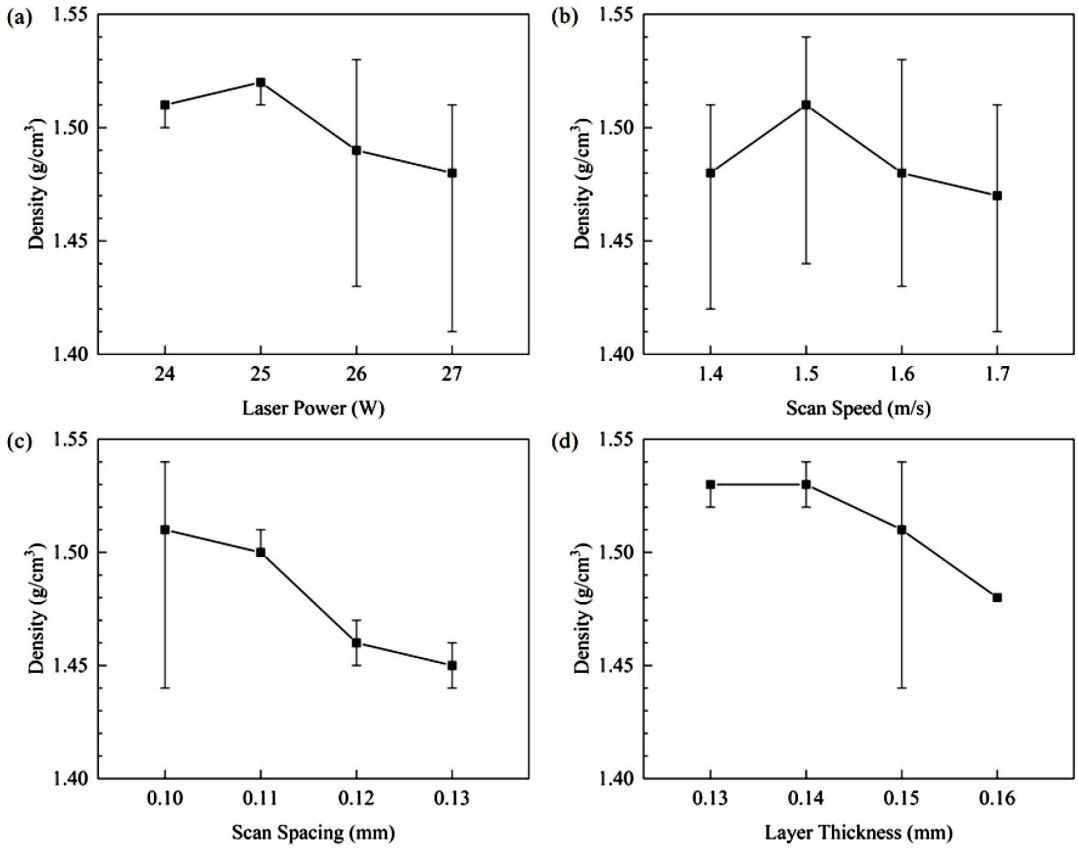

Figure 6. The effects of process parameters on density of PCSC parts: a) laser power, b) scanning speed, c) scanning spacing and d) layer thickness

Effects of process parameters on density

The effects of process parameters on the density of the PCSC parts are illustrated in Fig. 6. From Fig. 6a, it can be observed that as the laser power increases, the absorbed laser energy by PCSC powder increases, resulting in complete PF melting and a reduction in the number of internal voids within the PCSC parts. Consequently, the density of the PCSC parts increases. However, with the higher laser power, the laser energy transports further in the PCSC powder bed. More surrounding powder is sintered together, but the laser energy which transports to the surrounding powder is not high enough. Thus, the density of the surrounding part is lower than that of the main part, leading to the decrease in the density of the whole part.

From Fig. 6b, it can be observed that as the scanning speed increases, the laser beam spends less time on the powder bed, resulting in a decrease in the laser energy absorbed by the PCSC powder. Consequently, the PF is not completely melted, leading to an increase in the number of internal voids within the PCSC parts. Therefore, the density of PCSC parts decreases. However, with the lowering of the scanning speed, the laser remains on the powder bed for more time. Like the effect of the laser power, the laser energy transports further in the powder bed and more surrounding powder is sintered together, leading to a decrease in the density of the whole part.

From Fig. 6c, it can be observed that as the scan spacing increases, the remelting zone of the PCSC powder decreases. Consequently, the absorbed power by the powder gradually decreases, resulting in incomplete PF melting and a gradual increase in the number of internal voids. Consequently, the density of the PCSC parts decreases. From Fig. 6d, it can be observed that with an increase in layer thickness, the energy absorbed in the interlayer bonding region decreases, leading to an increase in the number of internal voids within the PCSC parts. Therefore, the density of the PCSC parts decreases.

SEM micrographs of the densified samples by varying laser power are shown in Fig. 7. It can be seen that when the laser power was 24 W, the internal voids are large and their amount was also large. With the laser power increasing, more PF melts and connects the SiC particles. The voids become smaller and their amount decreases.

Effects of process parameters on dimensional accuracies

The effects of process parameters on the dimensional accuracies of the PCSC parts in the *X*, *Y* and *Z* directions are illustrated in Fig. 8. From Fig. 8a, it can be observed that as the laser power increases, the power absorbed by the powder bed increases. As a result, the power transports throughout the powder bed. With the SLS pro-

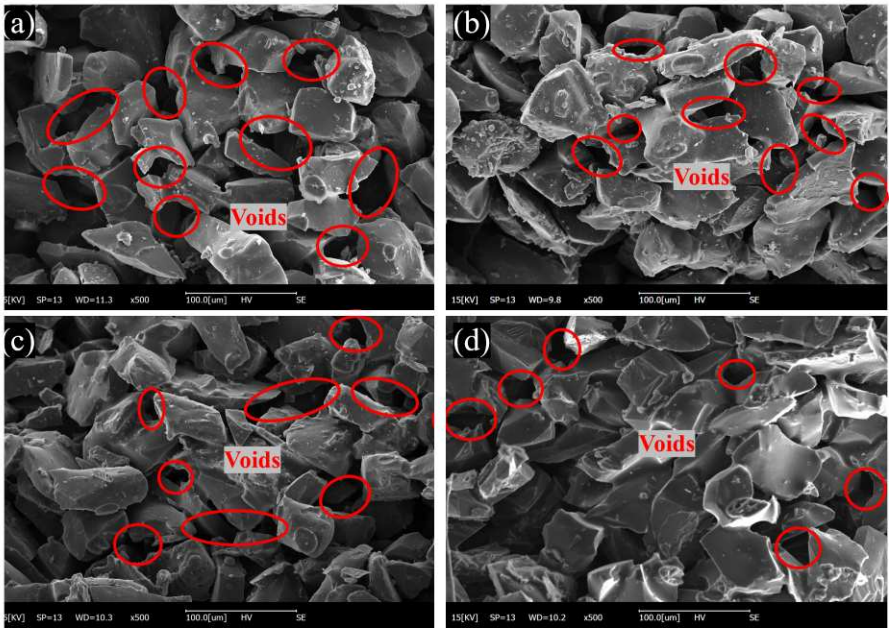

Figure 7. SEM micrographs of the densified samples under different laser power of: a) 24 W, b) 25 W, c) 26 W and d) 27 W

cess continuing, the heat accumulates in the powder bed and the heat inside is higher than that on the surface. Thus, the energy transports further along the direction of layer thickness. Consequently, the *Z*-dimensional accuracy decreases. When the laser power is high, it becomes difficult for the power to continue diffusing along the *X*-*Y* plane along the laser sintering path. However, in the *Z* direction, due to the accumulated heat in the powder bed, energy transport is more facilitated. Therefore, the dimensional accuracies in the *X* and *Y* directions are less affected, while the *Z*-dimensional accuracy continues to decrease with increasing laser power.

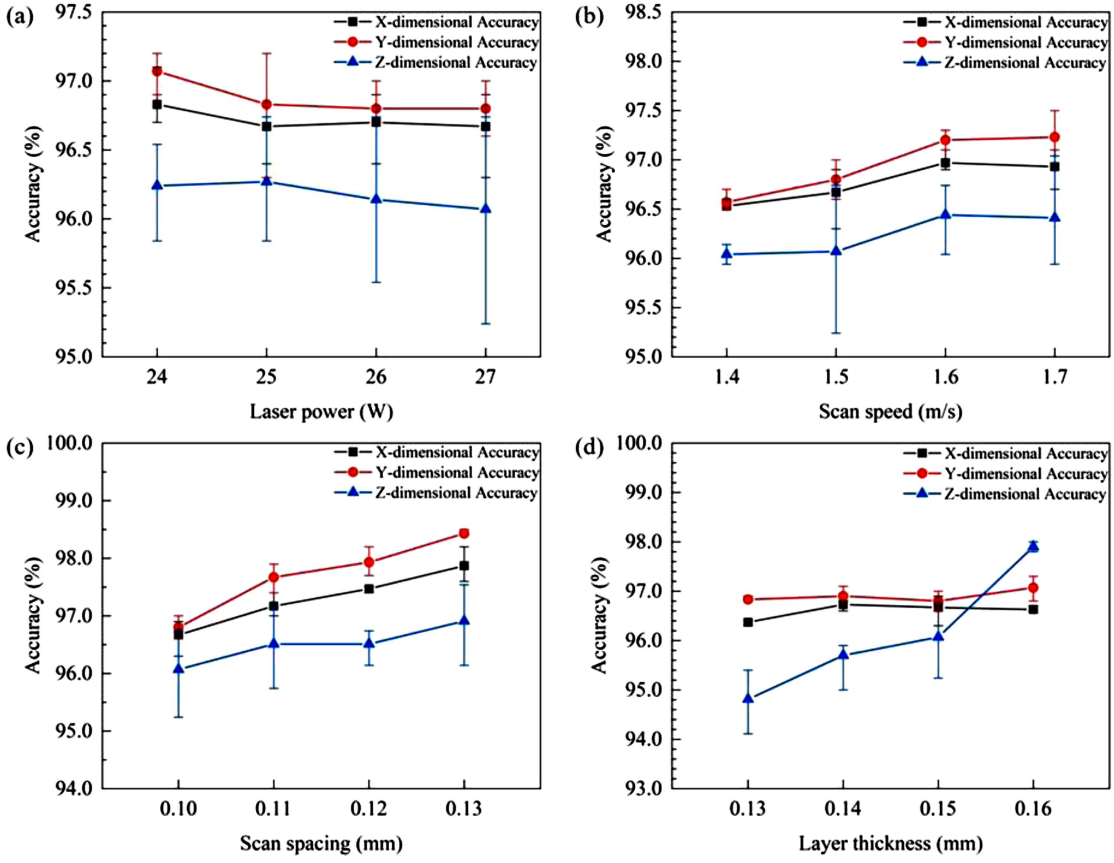

Figure 8. The effects of process parameters on *X*, *Y* and *Z*-dimensional accuracy of PCSC parts: a) laser power, b) scanning speed, c) scanning spacing and d) layer thickness

From Fig. 8b, it can be observed that as the scanning speed increases, the power absorbed by the powder bed decreases. This reduction in absorbed power limits the energy transport along the laser sintering path, resulting in a decrease in the dimensions in the *X*, *Y* and *Z* directions, thus improving the dimensional accuracies in all three directions. However, when the scanning speed reaches 1.6 m/s, further improvement in dimensional accuracies becomes difficult to achieve.

From Fig. 8c, it can be observed that as the scan spacing increases, the remelting zone decreases, resulting in reduced energy transport along the sintering path. This decrease in sintering depth improves the dimensional accuracies in the *X*, *Y* and *Z* directions. From Fig. 8d, it can be seen that, under a constant laser power, an increase in layer thickness leads to a reduction in the remelting zone between layers and a decrease in sintering depth. Consequently, the dimension in the *Z* direction of the sintered part decreases, thereby improving the *Z*-dimensional accuracy. However, the dimensional accuracies in the *X* and *Y* directions are less affected by changes in layer thickness.

3.3. Multi-index synthetic analysis

Synthetic weighted evaluation

The density and the dimensional accuracies in the *X*, *Y* and *Z* directions are four evaluation indicators considered in this analysis. The multi-index test results are evaluated using a comprehensive weighted scoring method. The comprehensive weighted scoring method determines the weights of multiple indicators based on the importance of each test indicator in the entire test. The multi-index test results are then converted into single index test results and the test plan is optimized based on the single index analysis method.

Dimensionless test index

The density and the dimensional accuracies in the *X*, *Y* and *Z* directions were transformed to dimensionless forms. The transformations were performed in accordance with Eqs. 3–6 [28]:

$$Z_1 = \frac{z_1 - z_{min}}{z_{max} - z_{min}} \tag{3}$$

$$Z_2 = \frac{z_2 - z_{min}}{z_{max} - z_{min}} \tag{4}$$

$$Z_3 = \frac{z_3 - z_{min}}{z_{max} - z_{min}} \tag{5}$$

$$Z_4 = \frac{z_4 - z_{min}}{z_{max} - z_{min}} \tag{6}$$

where z_1, z_2, z_3 and z_4 are respectively density, *X*-dimensional accuracy, *Y*-dimensional accuracy and *Z*-dimensional accuracy, and Z_1, Z_2, Z_3 and Z_4 are respectively dimensionless forms of density, *X*-dimensional accuracy, *Y*-dimensional accuracy and *Z*-dimensional accuracy.

Synthetic weights of test index

The greater the density of PCSC sintered parts, the denser the internal structure of the parts. The higher the dimensional accuracies, the higher the forming accuracy is. Based on the importance of the test index, the weight of the test indicators is given. Generally, the weight of the index with higher subjective importance is larger and the weight of the index with lower subjective importance is smaller.

The density and the *Z*-dimensional accuracy are key factors. The weights of density and the dimensional accuracies in the *X*, *Y* and *Z* directions are $\lambda_1 = 0.3$, $\lambda_2 = 0.2$, $\lambda_3 = 0.2$, and $\lambda_4 = 0.3$, respectively. Therefore, the synthetic weighted score is shown in Eq. 7 [28]:

$$Z = \lambda_1 Z_1 + \lambda_2 Z_2 + \lambda_3 Z_3 + \lambda_4 Z_4 \tag{7}$$

where *Z* is the synthetic weight.

Results and analysis of the test

Test data were processed by the synthetic weighted scoring method. The range analysis results of density and the dimensional accuracies in the *X*, *Y* and *Z* directions were obtained, as shown in Table 3.

In the Table 3, K_i represents the mean value of the synthetic weights of the corresponding test results when the level number on any column is *i*, and *R* is the range of the corresponding K_i. The level numbers refer to Table 2.

According to Table 3, parameter *D* exhibits the largest range which is 0.37, indicating the highest impact on the test index. Level 4 is deemed suitable for parameter *D*, because K_4 of parameter *D* is the largest [29]. In comparison, parameter *C* has a smaller range which is 0.20 than parameter *D*, and level 3 is considered appropriate for parameter *C*, because K_3 of parameter *C* is the largest. Similarly, parameter *A* has a smaller range which is 0.14 than parameter *B*, and level 3 is suitable for parameter *A*. Finally, parameter *B* has the smallest range which is 0.11, and level 4 is suitable for parameter *B*. Consequently, the optimal combination of factors is D4-C3-A3-B4, indicating a laser power of 25 W, a scanning speed of 1.7 m/s, a scanning spacing of 0.12 mm and a layer thickness of 0.16 mm. This optimization aims to enhance the density and dimensional accuracies in the *X*, *Y* and *Z* directions of the PCSC parts, as well as to improve the dimensional accuracies of the final SiC parts. It provides a foundation for selecting SLS process parameters and establishes a new direction for subsequent SLS tests of SiC composite powders.

The density of the PCSC parts sintered using optimized SLS process parameters reached 1.50 g/cm^3, with dimensional accuracies of 96.23% in the *X* direction, 96.80% in the *Y* direction, and 96.77% in the *Z* direction. After curing process and the carbonization pyrolysis reaction, the density increased to 1.51 g/cm^3, with dimensional accuracies of 97.23% in the *X* direction,

Table 3. SLS orthogonal experiment design and test results

Serial number	Laser power, A [W]	Scanning speed, B [m/s]	Scanning spacing, C [mm]	Layer thickness, D [mm]	Test index				
					Density [g/cm^3]	*X*-dimensional accuracy [%]	*Y*-dimensional accuracy [%]	*Z*-dimensional accuracy [%]	Synthetic weights
1	23	1.4	0.10	0.13	1.46	96.92	96.74	93.31	0.33
2	23	1.5	0.11	0.14	1.45	96.94	97.14	94.75	0.38
3	23	1.6	0.12	0.15	1.47	97.50	97.32	97.36	0.78
4	23	1.7	0.13	0.16	1.47	97.60	98.15	98.55	0.95
5	24	1.4	0.11	0.15	1.48	97.22	97.06	96.76	0.70
6	24	1.5	0.10	0.16	1.43	97.17	97.50	94.50	0.38
7	24	1.6	0.13	0.13	1.43	96.48	97.76	92.83	0.20
8	24	1.7	0.12	0.14	1.47	97.24	97.24	95.86	0.64
9	25	1.4	0.12	0.16	1.46	97.38	97.52	97.68	0.71
10	25	1.5	0.13	0.15	1.47	97.56	97.94	96.46	0.82
11	25	1.6	0.10	0.14	1.46	97.18	97.30	95.22	0.56
12	25	1.7	0.11	0.13	1.47	96.78	97.26	92.39	0.40
13	26	1.4	0.13	0.14	1.45	97.06	97.82	95.38	0.54
14	26	1.5	0.12	0.13	1.47	97.10	97.30	91.49	0.41
15	26	1.6	0.11	0.16	1.46	97.54	97.58	97.10	0.76
16	26	1.7	0.10	0.15	1.46	96.80	97.40	95.18	0.47
K_1	0.60	0.57	0.43	0.33					
K_2	0.48	0.50	0.56	0.53					
K_3	0.62	0.58	0.63	0.69	Optimal combination: D4-C3-A3-B4				
K_4	0.54	0.61	0.62	0.70					
R	0.14	0.11	0.20	0.37					

97.87% in the *Y* direction and 98.38% in the *Z* direction. The shrinkage rates in the *X*, *Y* and *Z* directions were measured to be 0.96%, 1.02% and 1.55%, respectively.

Figure 9 illustrates that the SiC particles are encapsulated by the PF binder, and the curing PCSC parts exhibit a dark brown colour due to the deepening of the colour after the curing process of PF. The PCSC parts exhibit clear contours, excellent surface quality and high dimensional accuracy. They can serve as precursors for complex SiC ceramic parts, facilitating structural modifications and shortening the product development cycle.

Figure 9. PCSC part after curing process

IV. Conclusions

In this study, phenol-formaldehyde-coated silicon carbide composite (PCSC) was prepared using hot coating method and a SiC precursor was formed using SLS technique. The test results of the experimental sintered parts showed that the processing parameters had a significant effect on the density and the dimensional accuracies in the *X*, *Y* and *Z* directions of the PCSC parts.

Through an orthogonal experiment of four factors and four levels, the effects and influence of the process parameters on PCSC parts are as follows (from larger to smaller): layer thickness > scan spacing > laser power > scanning speed. The optimal combination of various factors was D4-C3-A3-B4, namely, laser power was 25 W, scanning speed was 1.7 mm/s, scan spacing was 0.12 mm and layer thickness was 0.16 mm.

The density of the PCSC parts reached 1.50 g/cm^3, using the optimized process parameters in SLS, and the dimensional accuracies in the *X*, *Y* and *Z* directions

reached 96.23%, 96.80% and 96.77%, respectively. After curing process and the carbonization pyrolysis reaction, the density increased to 1.51 g/cm^3, with dimensional accuracies of 97.23% in the *X* direction, 97.87% in the *Y* direction and 98.38% in the *Z* direction. The shrinkage rates in the *X*, *Y* and *Z* directions were measured to be 0.96%, 1.02% and 1.55%, respectively.

Acknowledgements: The listed authors are grateful to the Natural Science Foundation of China, the Research and Development Center of 3D Printing Material and Technology of Northeast Forestry University. The authors disclosed receipt of the following financial support for the research, authorship, and/or publication of this article: The work was supported by the National Natural Science Fund of China under Grant number 52075090; the Key R&D Program of Heilongjiang Province under Grant number GA21A403; the Fundamental Research Funds for the Central Universities under Grant number 2572021BF01; and the Natural Science Foundation of Heilongjiang Province under Grant number YQ2021E002.

References

1. X. Wang, X. Gao, Z. Zhang, L. Cheng, H. Ma, W. Yang, "Advances in modifications and high-temperature applications of silicon carbide ceramic matrix composites in aerospace: A focused review", *J. Eur. Ceram. Soc.*, **41** [9] (2021) 4671–4688.
2. J. Du, H. Zhang, Y. Geng, W. Ming, W. He, J. Ma, Y. Cao, X. Li, K. Liu, "A review on machining of carbon fiber reinforced ceramic matrix composites", *Ceram. Int.*, **45** [15] (2019) 18155–18166.
3. T. Kimoto, J.A. Cooper, *Fundamentals of Silicon Carbide Technology: Growth, Characterization, Devices and Applications*, John Wiley & Sons, Singapore, 2014.
4. D. Han, H. Mei, S. Xiao, K.G. Dassios, L. Cheng, "A review on the processing technologies of carbon nanotube/silicon carbide composites", *J. Eur. Ceram. Soc.*, **38** [11] (2018) 3695–3708.
5. C. Liu, L. Cheng, H. Mei, X. Luan, "Influence of oxidation on fatigue life of a carbon/silicon carbide composite in water vapor containing environments", *Ceram. Int.*, **35** [4] (2009) 1397–1402.
6. J. Ramírez-Rico, M. Singh, D. Zhu, J. Martínez-Fernández, "High-temperature thermal conductivity of biomorphic SiC/Si ceramics", *J. Mater. Sci.*, **52** [17] (2017) 10038–10046.
7. D. Grossin, A. Montón, P. Navarrete-Segado, E. Özmen, G. Urruth, F. Maury, D. Maury, C. Frances, M. Tourbin, P. Lenormand, G. Bertrand, "A review of additive manufacturing of ceramics by powder bed selective laser processing (sintering/melting): Calcium phosphate, silicon carbide, zirconia, alumina, and their composites", *Open Ceram.*, **5** (2021) 100073.
8. K. Zhang, T. Zeng, G. Xu, S. Cheng, S. Yu, "Mechanical properties of SiCp/SiC composite lattice core sandwich panels fabricated by 3D printing combined with precursor impregnation and pyrolysis", *Compos. Struct.*, **240** (2020) 112060.
9. T. Koyanagi, K. Terrani, S. Harrison, J. Liu, Y. Katoh, "Additive manufacturing of silicon carbide for nuclear applications", *J. Nucl. Mater.*, **543** (2021) 152577.
10. W. Wu, Y. Zou, C. Li, Y.-W. Li, Z. Wang, N. Chang, Y. Shi, "Effect of impregnated phenolic resin on the properties of Si–SiC ceramic matrix composites fabricated by SLS-RMI", *Ceram. Int.*, **49** [2] (2023) 1624–1635.
11. J. Li, A.I. Bolad, Y. Guo, Y. Wang, E.A. Elfaki, S.A.A. Adam, G.A.A.M. Ahmed, "Effects of various processing parameters on the mechanical properties and dimensional accuracies of *Prosopis chilensis*/PES composites produced by SLS", *Rapid Prototyping J.*, **28** [6] (2022) 1144–1167.
12. D. Zhao, Y. Guo, K. Jiang, H. Zhang, "Preparation and selective laser sintering of bamboo flour/copolyester composite and post-processing", *J. Thermoplast. Compos. Mater.*, **30** [8] (2015) 1045–1055.
13. Z. Chen, Z. Li, J. Li, C. Liu, C. Lao, Y. Fu, C. Liu, Y. Li, P. Wang, Y. He, "3D printing of ceramics: A review", *J. Eur. Ceram. Soc.*, **39** [4] (2019) 661–687.
14. A. Jayswal, S. Adanur, "Characterization of polylactic acid/thermoplastic polyurethane composite filaments manufactured for additive manufacturing with fused deposition modelling", *J. Thermoplast. Compos. Mater.*, **36** [4] (2021) 1450–1471.
15. J. Wang, S.R. Sama, P.C. Lynch, G. Manogharan, "Design and topology optimization of 3D-printed wax patterns for rapid investment casting", *Procedia Manufactur.*, **34** (2019) 683–694.
16. W. Zeng, Y. Guo, K. Jiang, Z. Yu, Y. Liu, Y. Shen, J. Deng, P. Wang, "Laser intensity effect on mechanical properties of wood-plastic composite parts fabricated by selective laser sintering", *J. Thermoplast. Compos. Mater.*, **26** [1] (2012) 125–136.
17. R. Deckard Carl, "Method and apparatus for producing parts by selective sintering". *US patent US 4863538 A*, 1989.
18. R. Deckard Carl, "Apparatus for producing parts by selective sintering". *US patent US 5597589 A*, 1997.
19. Y. Shi, J. Chen, Y. Wang, Z. Li, S. Huang, "Study of the selective laser sintering of polycarbonate and postprocess for parts reinforcement", *Proceed. Institution of Mechanical Engineers, Part L: J. Mater.: Design Appl.*, **221** [1] (2007) 37–42.
20. G. Özer, B. Özbay, Z.Ç. Öter, G. Tarakçi, M.S. Yılmaz, M.E. Bulduk, E. Koç, S. Acar, K.A. Güler, "Investigation of the surface quality and dimensional accuracy of polymer patterns produced by selective laser sintering (SLS) method for investment casting (IC)", *Int. J. Cast Metals Res.*, **33** [2-3] (2020) 146–152.
21. H. Fu, W. Zhu, Z. Xu, P. Chen, C. Yan, K. Zhou, Y. Shi, "Effect of silicon addition on the microstructure, mechanical and thermal properties of Cf/SiC composite prepared via selective laser sintering", *J. Alloys Compd.*, **792** (2019) 1045–1053.
22. L. Jin, K. Zhang, T. Xu, T. Zeng, S. Cheng, "The fabrication and mechanical properties of SiC/SiC composites prepared by SLS combined with PIP", *Ceram. Int.*, **44** [17] (2018) 20992–20999.
23. S. Meyers, "Additive manufacturing of technical ceramics: Laser sintering of alumina and silicon carbide", *Ph.D. Thesis*, KU Leuven, Faculty of Engineering Science, Belgium, 2019.
24. J.C. Nelson, N.K. Vail, J.W. Barlow, J.J. Beaman, D.L. Bourell, H.L.J.I. Marcus, "Selective laser sintering of

polymer-coated silicon carbide powders", *Ind. Eng. Chem. Res.*, **34** [5] (1995) 1641–1651.
25. W. Zhu, H. Fu, Z. Xu, R. Liu, P. Jiang, X. Shao, Y. Shi, C. Yan, "Fabrication and characterization of carbon fiber reinforced SiC ceramic matrix composites based on 3D printing technology", *J. Eur. Ceram. Soc.*, **38** [14] (2018) 4604–4613.
26. K. Liu, T. Wu, D.L. Bourell, Y. Tan, J. Wang, M. He, H. Sun, Y. Shi, J. Chen, "Laser additive manufacturing and homogeneous densification of complicated shape SiC ceramic parts", *Ceram. Int.*, **44** [17] (2018) 21067–21075.
27. S. Song, Z. Gao, B. Lu, C. Bao, B. Zheng, L. Wang, "Performance optimization of complicated structural SiC/Si composite ceramics prepared by selective laser sintering", *Ceram. Int.*, **46** [1] (2020) 568–575.
28. Y. Zhuang, Y. Guo, J. Li, Y. Yu, K. Jiang, H. Zhang, S. Guo, "Study on the forming and sensing properties of laser-sintered TPU/CNT composites for plantar pressure sensors", *Int. J. Adv. Manufact. Technol.*, **112** [7] (2021) 2211–2222.
29. Y. Yu, Y. Guo, T. Jiang, J. Li, K. Jiang, H. Zhang, "Study on process and parameter optimization of selective laser sintering of walnut shell composite powder", *BioRes*, **13** [2] (2018) 3017–3029.